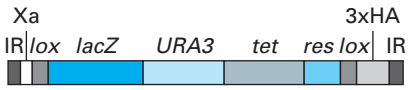

FIGURE 6.1 • Diagram of mTn. IR, inverted repeat; *lox,* a recombination site for excising intervening DNA; Xa, a restriction site; *lacZ,* a gene that encodes β-galactosidase; *URA3,* a gene required for uracil synthesis; *tet,* tetracycline resistance gene; *res,* required for transposition; 3xHA, three copies of the DNA encoding hemagglutinin epitope tag. To create the mutations, a yeast genomic plasmid library in *E. coli* was randomly mutagenized by insertion of mTn. Individual plasmid clones were isolated and used for homologous recombination to replace the *wt* gene with the mTn-mutated one in *URA3* lacking diploid strains.

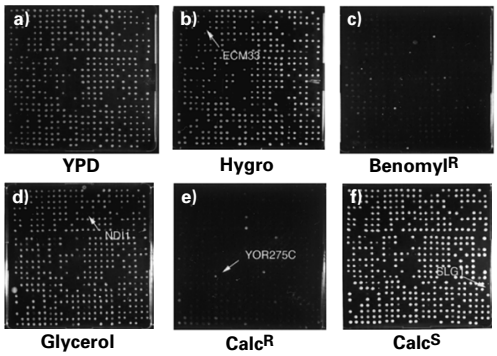

FIGURE 6.2 • Phenotype *macro*array analysis. Examples of 21 × 21 cm macroarrays testing growth on different media: **a)** YPD, **b)** YPD supplemented with 20 mg/ml benomyl, **c)** YPD with 69.7 mg/ml calcofluor, **d)** YPD with 46 mg/ml hygromycin, **e)** YPGlycerol, and **f)** YPD supplemented with 12 mg/ml calcofluor. Arrows indicate strains mutated for genes functioning in cellular respiration (*Ndi1*) or cell-wall biogenesis (*Ecm33, Slg1,* YOR275C).

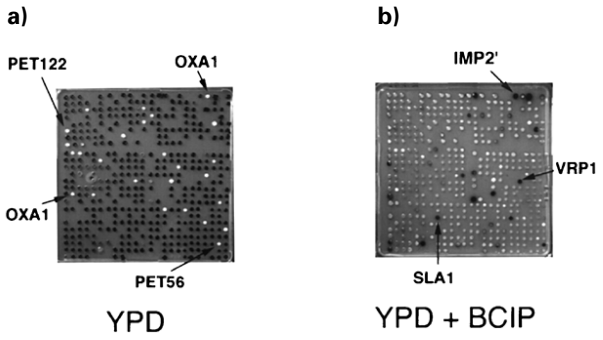

FIGURE 6.3 • Macroarray analysis of metabolic pathways. a) Metabolic mutants unable to carry out oxidative phosphorylation were identified as white (rather than red) colonies on YPD medium; all cells contained the *ade2* mutation, which leads to red pigment formation in *wt* metabolism. Respiratory genes identified by this method are labeled with arrows. **b)** Genes functioning in cell-wall maintenance were characterized through macroarray analysis of mutants grown on YPD overlaid with agar containing a mild detergent and BCIP. Dark colonies mark cells that lysed; arrows highlight genes known to be involved in cell-wall maintenance.

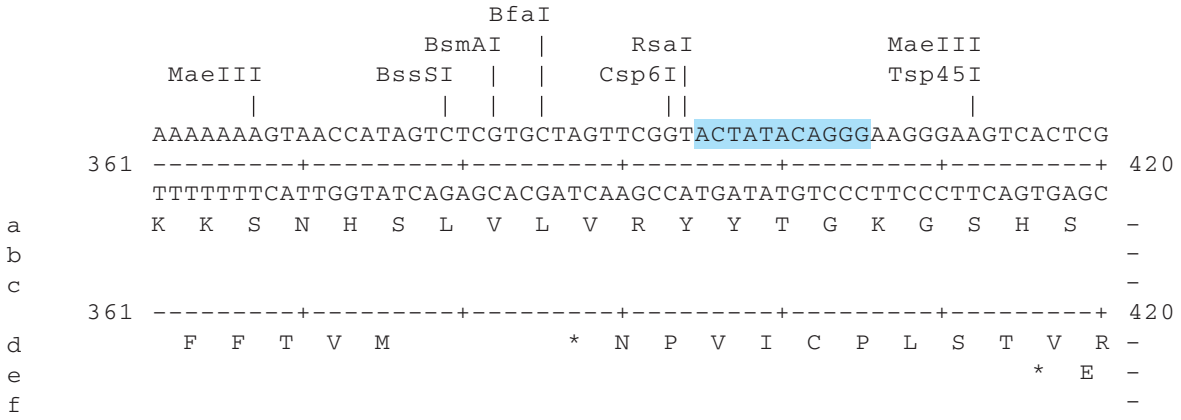

FIGURE 6.4 • Region of interest in yeast genome, including putative NORF. The site of mTn insertion is highlighted in blue. Above the double-stranded DNA sequence are restriction sites. Below the DNA are the six frames of translation (a, b, c top strand; d, e, f bottom strand) with a dashed line separating the three forward and reverse reading frames. Stars indicate stop codons.

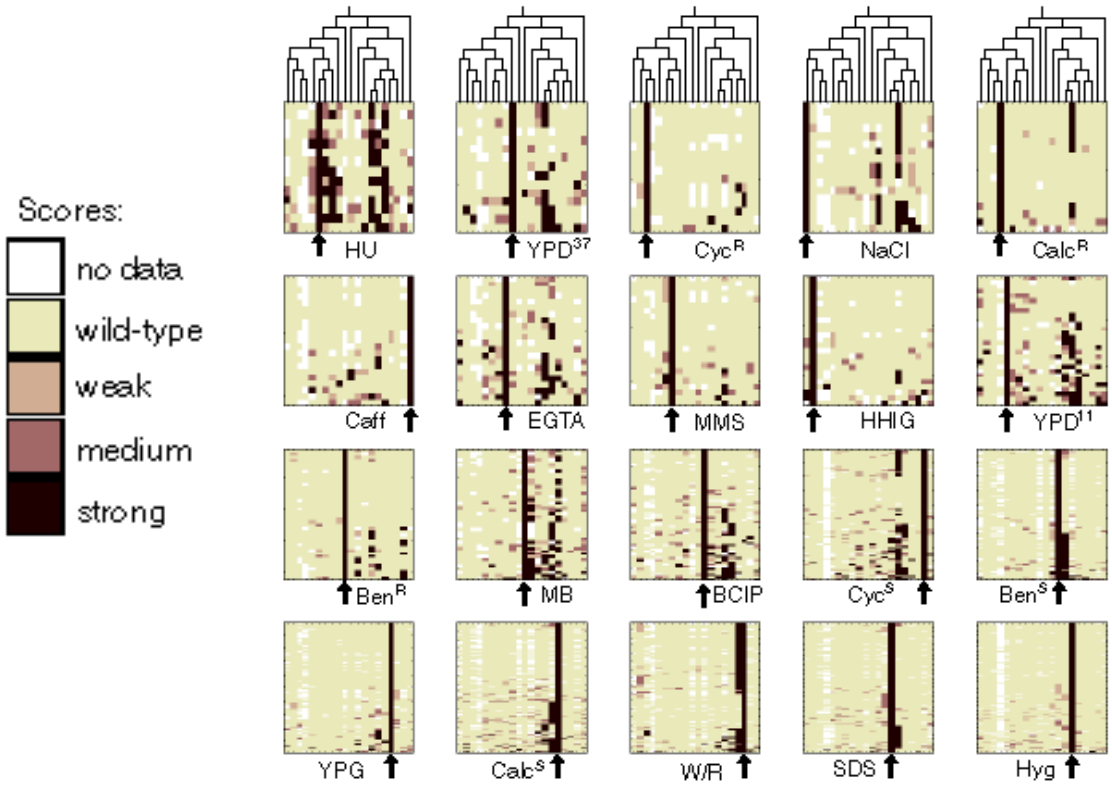

FIGURE 6.5 • Clustered microarray phenotype data. Sixteen phenotype clusters exhibit a predominant phenotype. Vertical columns represent growth conditions; horizontal rows represents a different strain; colors indicate strength of phenotype. Strains in each cluster were sorted from top to bottom according to the distance from the cluster average. Abbreviations below clusters indicate the predominant phenotype, and arrows point to the column representing this predominant phenotype. In addition to clustering strains (the rows of the data set), they also clustered vertical data columns (representing growth conditions). The dendrogram generated by column clustering is shown above the first row of clusters.

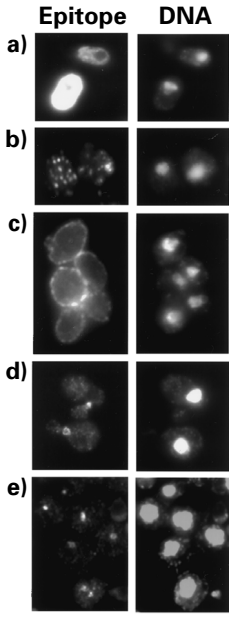

FIGURE 6.6 • Localization of epitope-tagged proteins. **(Left column)** Examples of immunofluorescence patterns in cells stained with monoclonal antibody against HA. **(Right column)** The same cells stained with a DNA-binding dye called DAPI. Numbers in parentheses indicate the number of strains with similar labeling patterns: **a)** Diffuse cytoplasmic labeling (189). **b)** A punctate pattern of cytoplasmic labeling (10) **c)** Localization to the plasma membrane. **d)** A ring in the mother-bud neck (2). **e)** The spindle body (5).

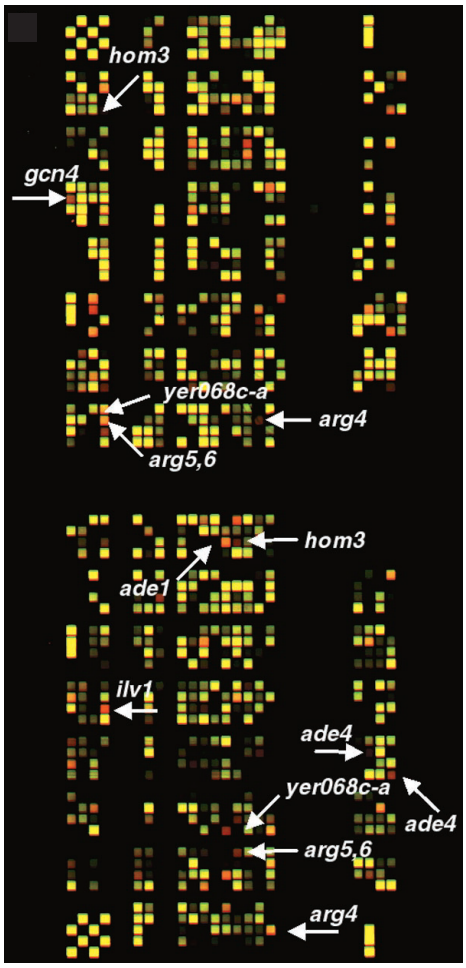

FIGURE 6.7 • Bar code microarray. a) To screen many cells simultaneously, many different mutants were incubated in a common flask of growth media (top). An aliquot of cells was used to produce the mixture of barcode PCR products that were coupled to a red dye. Two-color comparison of bar code microarray hybridized with fluorescently labeled PCR products amplified from genomic DNA extracted from 558 strains grown for 0 (red channel) or 6 hours (green channel) in minimal medium. Only a portion of the full microarray is shown. Strains that exhibit a growth defect in minimal medium are labeled.

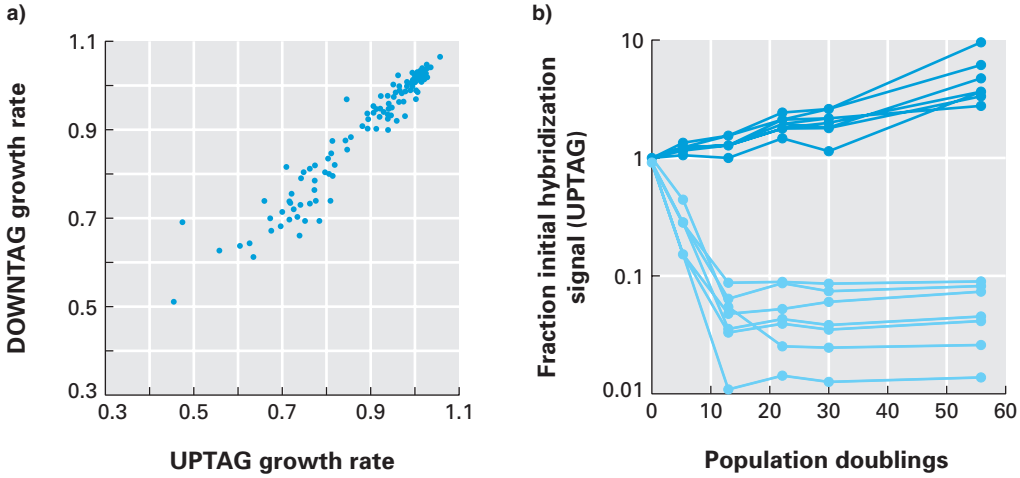

FIGURE 6.8 • Analysis of bar code DNA microarrays. **a)** Correlation of growth rate data obtained with both bar code (DOWNTAG and UPTAG) sequences for strains grown in rich medium. Data are shown for 331 strains that produced UPTAG and DOWNTAG hybridization signals that were both at least threefold over background at time zero. **b)** Normalized hybridization intensity data for the 10 slowest-growing (light blue) and 10 fastest-growing (dark blue) strains in rich medium. The data are presented as fraction of labeling intensity at time zero (log scale on Y-axis) over time in the form of population doubling (X-axis).

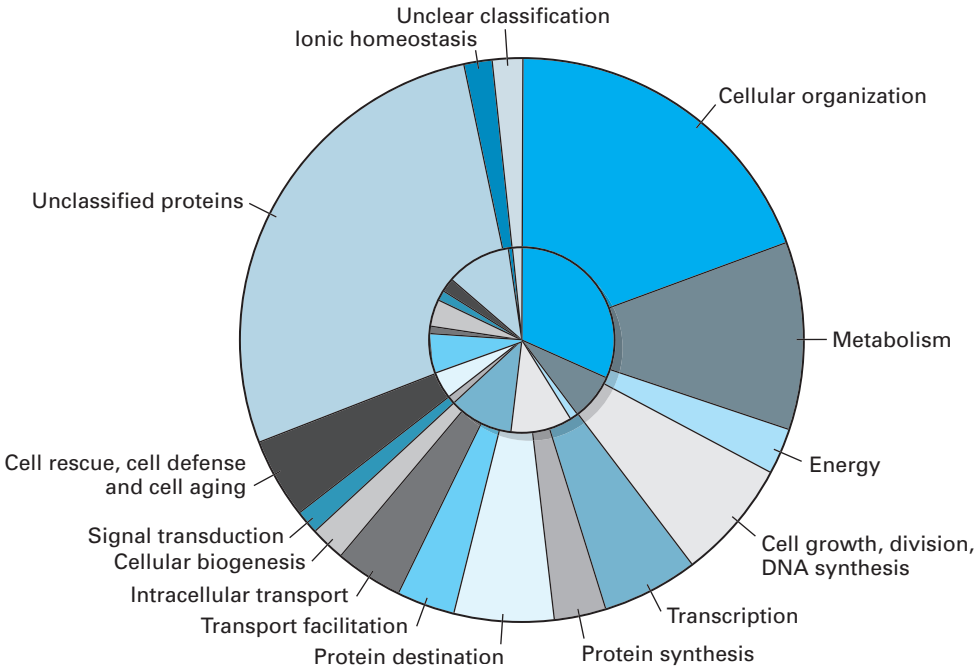

FIGURE 6.9 • Bar code analysis of biological processes. Distribution of functional classes of essential (inner circle) and nonessential (outer circle) genes using criteria from the Munich Information Center for Protein Sequences (MIPS).

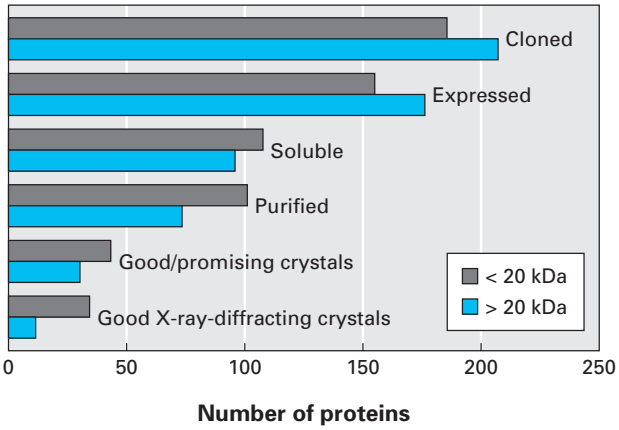

FIGURE 6.10 • Structural proteomics of an Archaea. Histograms of the number of *M. thermoautotrophicum* proteins at the end of each step in cloning, expression, and sample preparation. Proteins were divided into two classes based on molecular weight.

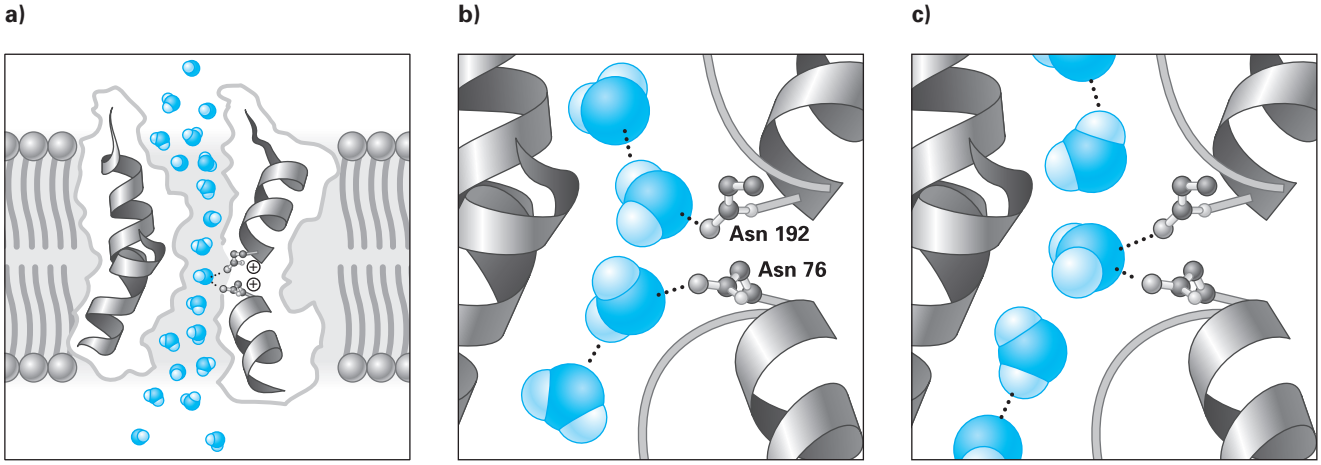

FIGURE 6.11 • Structural basis for aquaporin function. a) The charges from the helix control the orientation of the water molecules passing through the narrowest part of the channel. **b)** and **c)** The hydrogen bonding of a water molecule to asparagines 192 and 76, which extend their R groups to form the narrowest part of the channel.

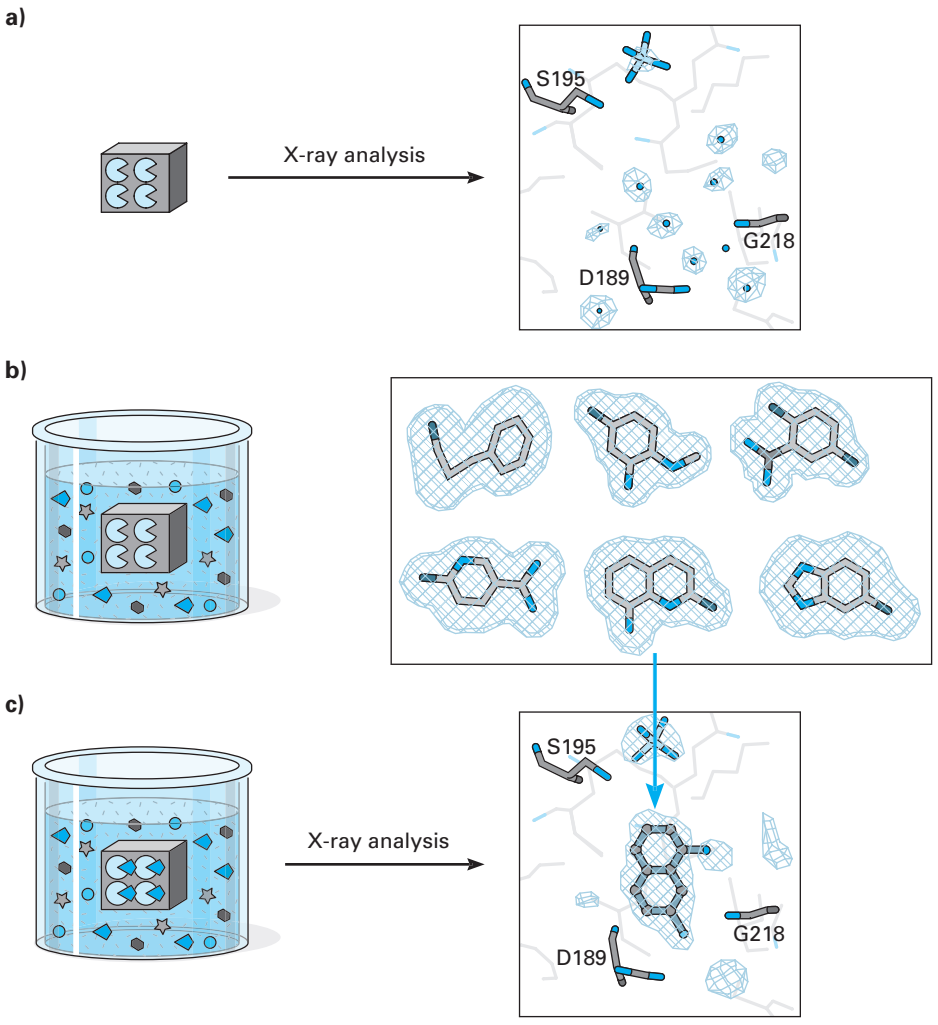

FIGURE 6.12 • Structural method to discover new medications. a) In an ideal situation, the active site is open to the solvent when the protein is crystallized. **b)** Different small molecules are mixed with the crystallized protein. **c)** Those with appropriate shapes will be incorporated into the crystal. In the structure web page of urokinase, you can see an inhibitor similar to aminopyrimidyl 2-aminoquinoline, which inhibits the enzyme at 0.37 μM.

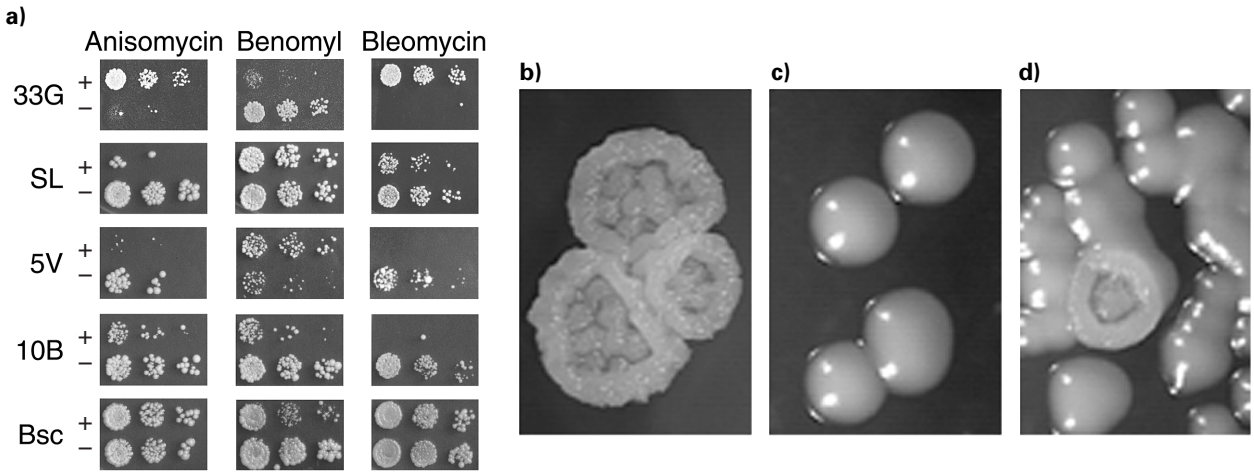

FIGURE 6.13 • Functional consequences of protein conformation. **a)** Sup35 prion conformation affects growth in different genetic backgrounds and under different conditions. Media contain fungicides anisomycin, benomyl, or bleomycin. Five different strains are grown in the presence of a prion-shaped Sup35 (+) or the absence of prion shape (−). **b)** Colony morphology is altered by prion conformation in Sup35. Cells were grown, diluted, and spotted onto plates containing potassium acetate and grown at 30°C. **c)** Cells lacking a prion form of Sup35 and **d)** the spontaneous appearance of a colony containing prion-shaped Sup35 amidst many colonies lacking prion-shaped Sup35.

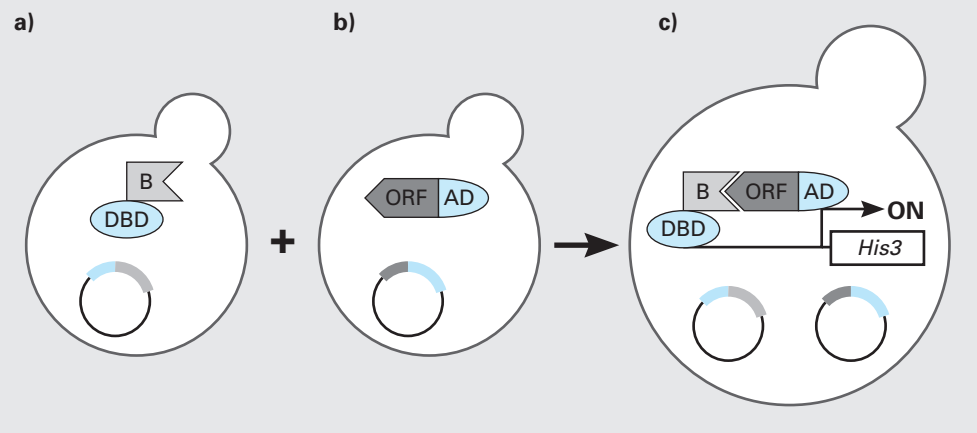

FIGURE 6.14 • Yeast two-hybrid method. a) The DNA binding domain (DBD) is fused onto the protein of interest "B." This construct, the "bait," is encoded by the plasmid shown in the same cell. **b)** The "prey" is encoded by its own plasmid and is composed of an ORF fused onto the activation domain (AD), which is capable of activating RNA polymerase. **c)** Both the bait and prey plasmids are inside the same cell, and if the B and ORF protein physically interact, the RNA polymerase will be able to transcribe a reporter gene, in this case *His3*.

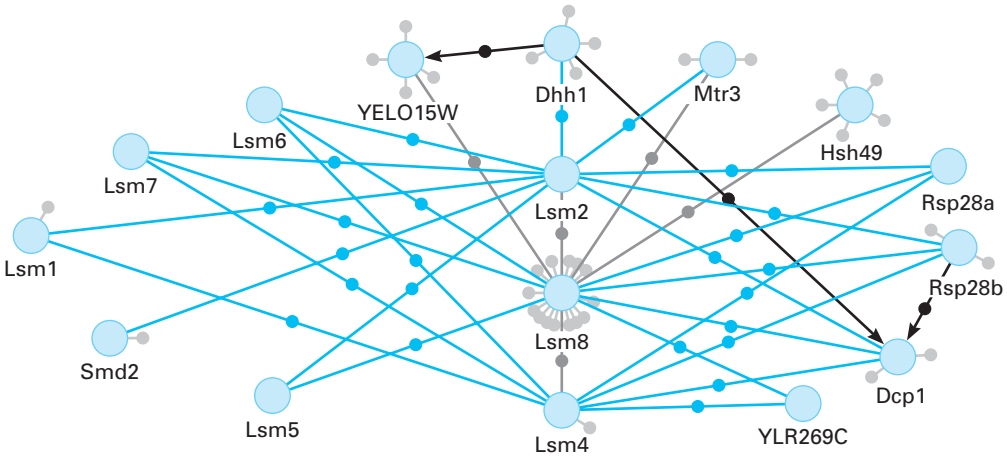

FIGURE 6.15 • Proteomics circuit showing the interactions of RNA splicing proteins. The proteins are indicated by large blue nodes and their interactions with lines. The dots on the lines help you follow each line. Blue lines show interactions that were detected by traditional Y2H array screens, black from multiple high-throughput screens, and gray from literature and array screens. The black arrows point away from the protein used as bait in the screens. Small gray nodes indicate other protein-protein interactions not highlighted here.

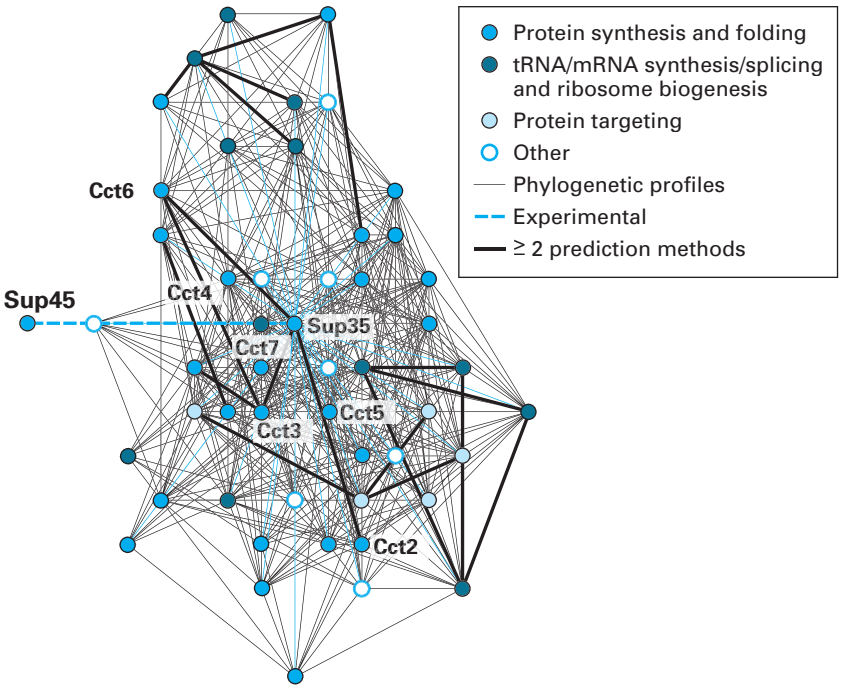

FIGURE 6.16 • Network of protein interactions with higher (bold lines) and lower (thin lines) confidence. This network is centered on the yeast prion protein Sup35. Many of the proteins in this network are involved in protein synthesis, including ribosomes, protein folding, sorting, modification, and targeting. To construct this model, proteins were treated as nodes and the edges as springs in order to position functionally related proteins close to each other.

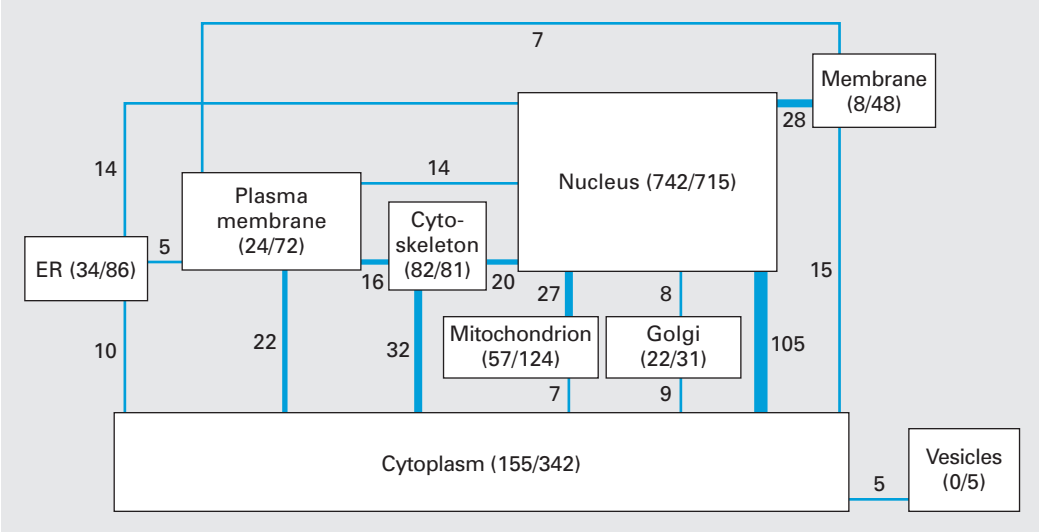

FIGURE 6.17 • Protein interactions grouped by cellular compartments. Numbers in parentheses indicate the number of interactions in the circuit diagram among proteins of this compartment/the total number of proteins in the same compartment. Lines connecting compartments indicate the number of protein interactions by the thickness of each line (numbers of connections are near each line). For example, there are 7 interactions between the 48 membrane proteins and the 72 plasma membrane proteins in "Benno Figure 1."

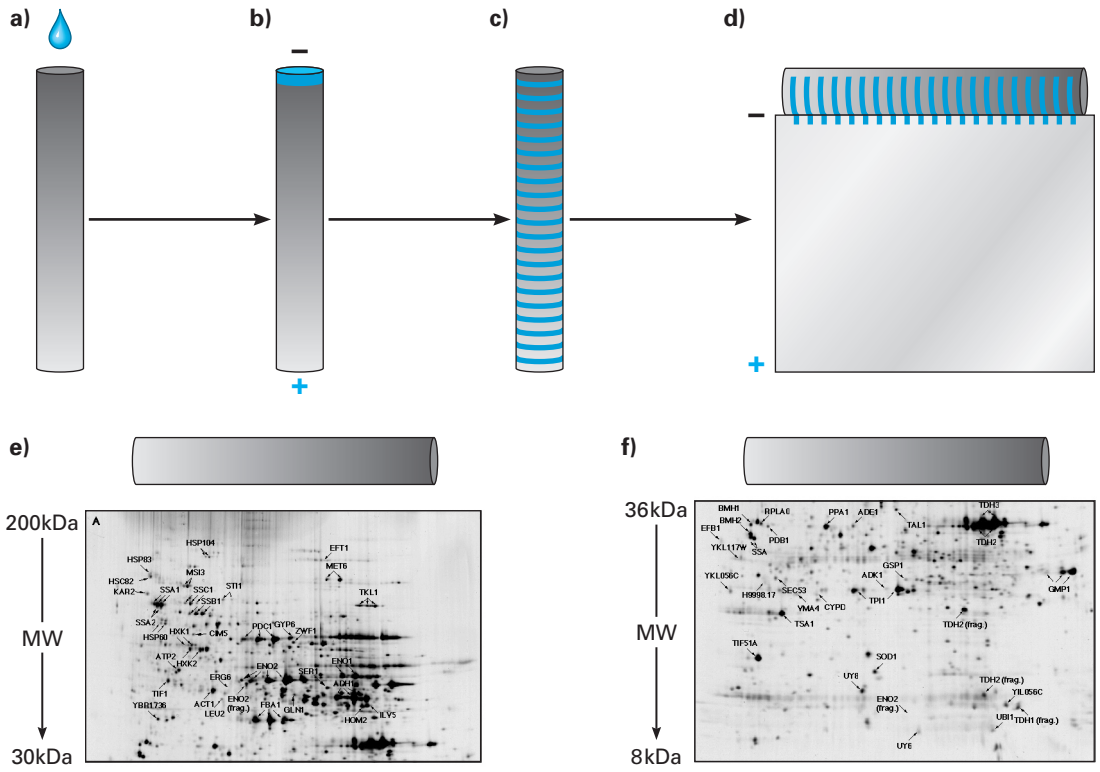

FIGURE 6.18 • Two-dimensional (2D) gel electrophoresis. Each column (a–c) with a gradation of gray shading represents the isoelectric focusing gel with a pH gradient. **a)** A mixture of proteins (blue drop) is applied to the isoelectric focusing gel and **b)** exposed to an electrical current. **c)** Proteins migrate to their isoelectric points (pI) and stop moving. **d)** This tubular gel is placed on top of a slab polyacrylamide gel that contains SDS and is subjected to electrophoresis (SDS-PAGE). Proteins migrate into the slab gel according to their molecular weights. Yeast cells were grown in rich media and subjected to 2D gel analysis. Using duplicate isoelectric focusing gels, large **e)** and small **f)** proteins were analyzed on separate gels. The same spots appear at the bottom of e) and the top of f). Molecular weights are resolved on the Y-axis and pIs on the X-axis. Panels e) and f) are from the Swiss 2D database at ExPASy.

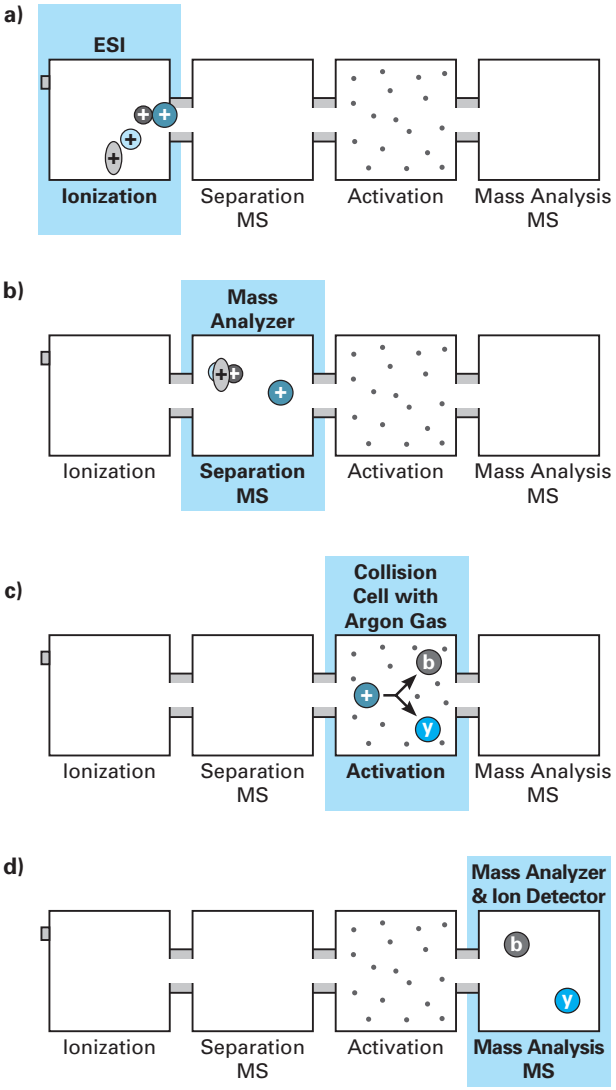

FIGURE 6.19 • Tandem mass spectrometry for protein identification. **a)** ESI creates ionized proteins, represented by the colored shapes with positive charges. Each shape represents many copies of identical proteins. **b)** The ionized proteins are separated based on their mass to charge ratio (m/z) and sent one at a time into the activation chamber. Separation and selection takes place in the first of the two MS devices. The solid blue protein has been selected for analysis while the other three are temporarily stored for later analysis. **c)** The group of m/z selected ionized proteins enters the collision cell that is filled with inert argon gas. The gas molecules collide with the proteins, which causes them to break into two peptide pieces (labeled b and y). **d)** Ionized peptide pieces are sent into the second MS device which again measures the m/z ratio. It is connected to a computer that compares this spectrum of peptide pieces to a database of ideal spectra to identify the original group of identical proteins.

a)

S–P–A–F–D–S–I–M–A–E–T–L–K
(protonated mass 1410.6)

Mass$^+$	b-ions	y-ions	Mass$^+$
81.1	S	PAFDSIMAETLK	1323.6
185.2	SP	AFDSIMAETLK	1226.4
256.3	SPA	FDSIMAETLK	1155.4
403.5	SPAF	DSIMAETLK	1008.2
518.5	SPAFD	SIMAETLK	893.1
605.6	SPAFDS	IMAETLK	806.0
718.8	SPAFDSI	MAETLK	692.3
850.0	SPAFDSIM	AETLK	561.7
921.1	SPAFDSIMA	ETLK	490.6
1050.2	SPAFDSIMAE	TLK	361.5
1151.3	SPAFDSIMAET	LK	260.4
1264.4	SPAFDSIMAETL	K	147.2

b)

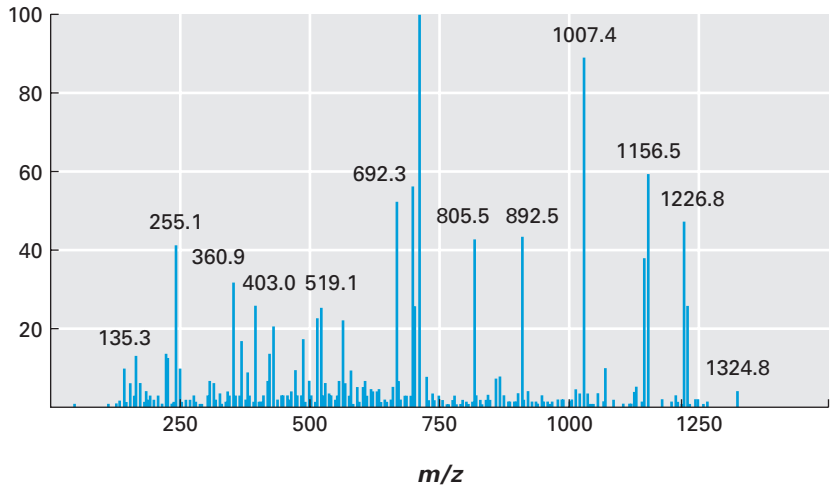

FIGURE 6.20 • Protein identification through peptide fragment formation and separation. When a group of identical proteins is broken into its peptide pieces, more than one pair of b and y peptides will be formed. **a)** One protein sequence and its calculated mass on top, with the b peptides/masses (gray) and the y peptides/masses (blue) below. **b)** An experimentally determined mass/charge spectrum from the peptide in a). Notice that some peaks are higher than others, which means that some b/y peptide pieces were more abundant than others. The spectrum is used to determine the peptide's amino acid sequence and protein identity.

FIGURE 6.21 • Phagosome 2D gel. Phagosomes were isolated from macrophages and subjected to isoelectric focusing (IEF) and SDS-PAGE. The pH gradient is presented above the gel and the molecular weight standards to the left. This gel was silver stained to locate the spots, which were excised and identified by tandem MS.

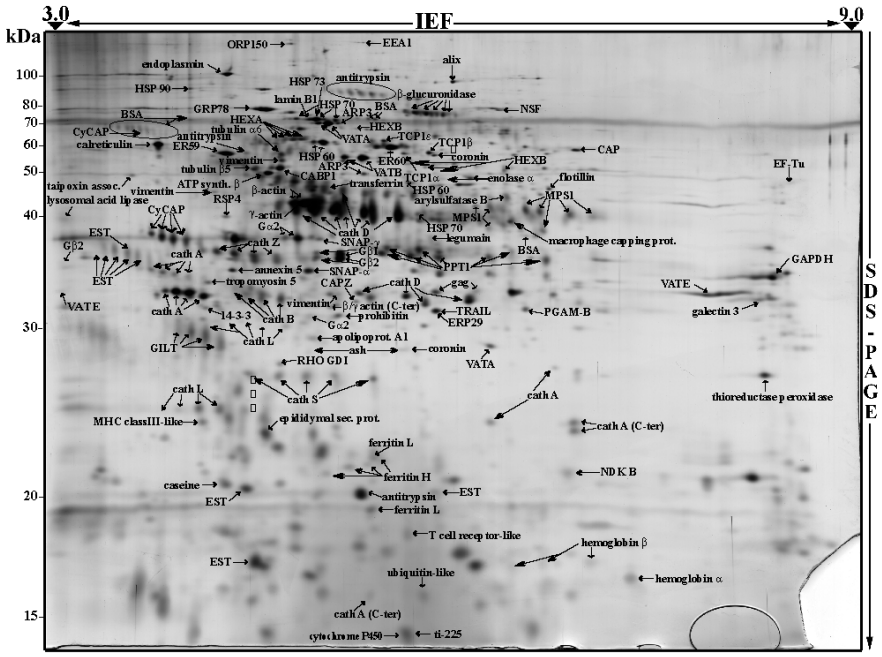

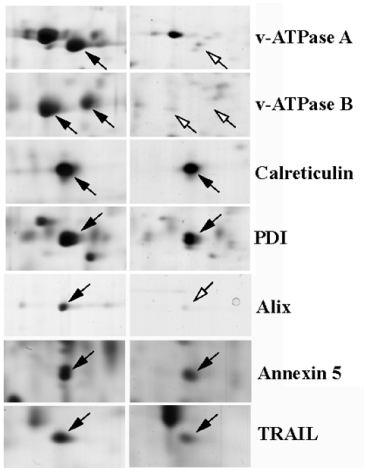

FIGURE 6.22 • Localization of phagosome proteins. Phagosomes were subjected to protease treatment to digest any proteins on the cytoplasmic side of the phagosome. Untreated (left) and protease-treated (right) phagosomes were compared on 2D gels. Proteins with substantial cytosolic portions are indicated with open arrows, while those resistant to protease are indicated with closed arrows.

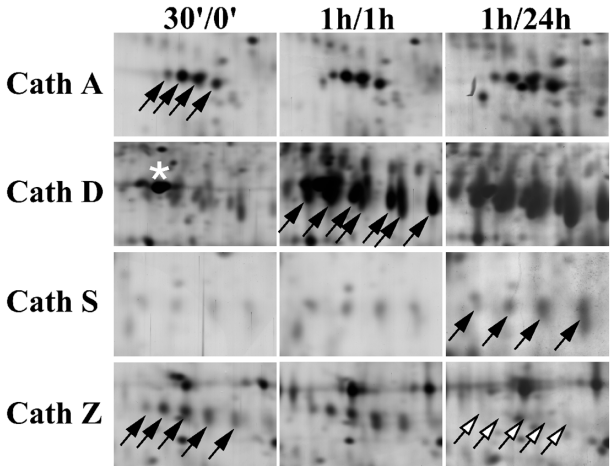

FIGURE 6.23 • Cathepsin composition during phagosome maturation. Phagosomes from macrophages were isolated after 30 minutes of exposure to latex beads (30'/0'), after 1 hour of incubation with latex beads followed by 1 hour of further development (1h/1h), or 1 hour of latex beads followed by 24 hours of further development (1h/24h). The cathepsins are labeled on the left, with loss of signal indicated by the open arrows. Multiple arrows point to the multiple spots for each cathepsin. The star denotes a precursor form of cathepsin D.

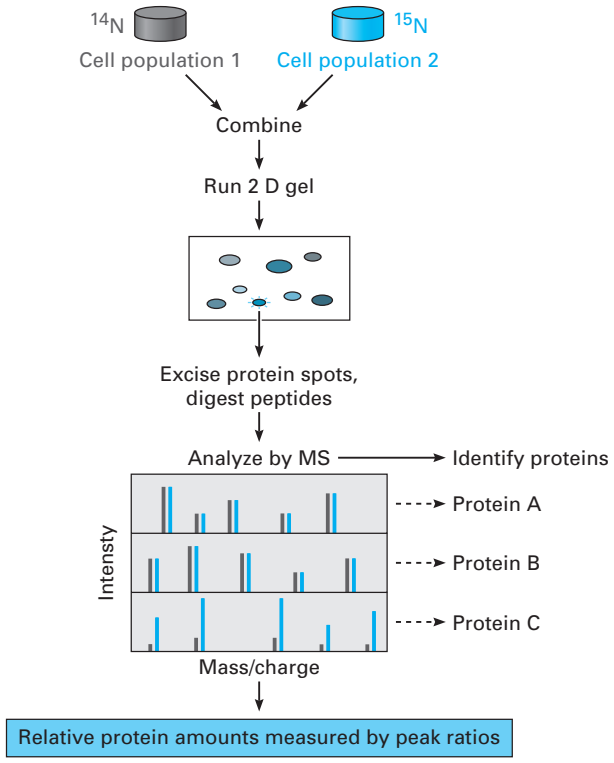

FIGURE 6.24 • Quantifying differences in proteomes. Two cell pools are grown in the presence (blue = cell population 2) or absence (gray = cell population 1) of heavy nitrogen ^{15}N. The proteins are extracted, pooled, and subjected to 2D gel analysis; spots excised; and proteins identified and quantified by MS/MS. The relative areas under the pairs of heavy and light peptide peaks indicate relative abundance of each protein pair.

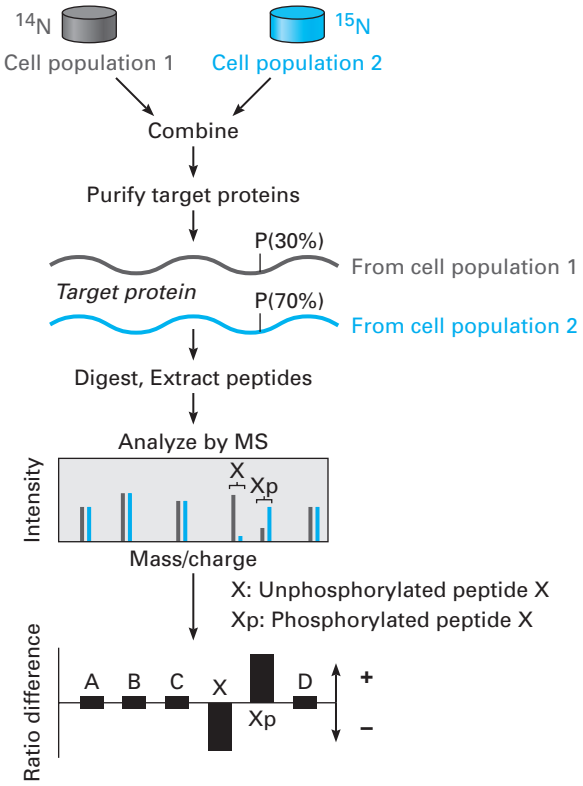

FIGURE 6.25 • Quantifying relative levels of phosphorylation. Bar graphs A, B, C, and D indicate no difference for proteins A–D in the two populations. Compared to population 1, unphosphorylated protein X was reduced in population 2. Phosphorylated protein X (Xp) was increased in population 2.

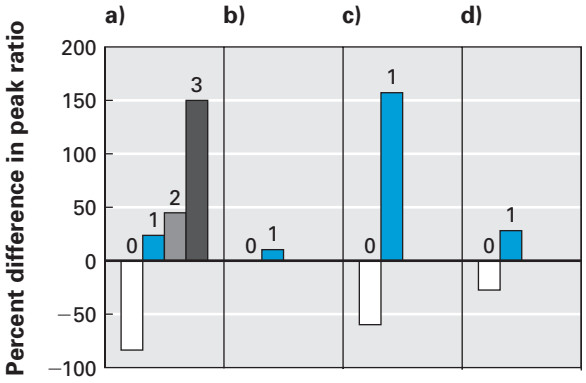

FIGURE 6.26 • Phosphorylation of Ste20 requires Cln2. Four Ste20 peptides are phosphorylated in *wt* cells but not *cln2* cells. The bar graphs show the loss of unphosphorylated Ste20 peptides (negative change) and the appearance of phosphorylated Ste20 peptides (positive change). The numbers above each bar indicate the number of phosphates added to each peptide.

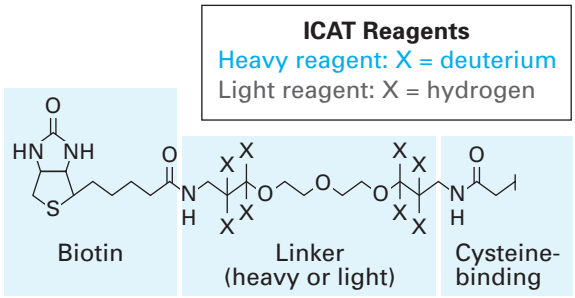

FIGURE 6.27 • ICAT labeling reagent. The reagent consists of three parts: an affinity tag in the form of biotin that binds irreversibly to avidin; a linker that contains eight stable isotopes; and a reactive group that will bind cysteines. The reagent exists in two forms: heavy contains eight deuterium atoms (blue), and light contains eight hydrogen atoms (gray).

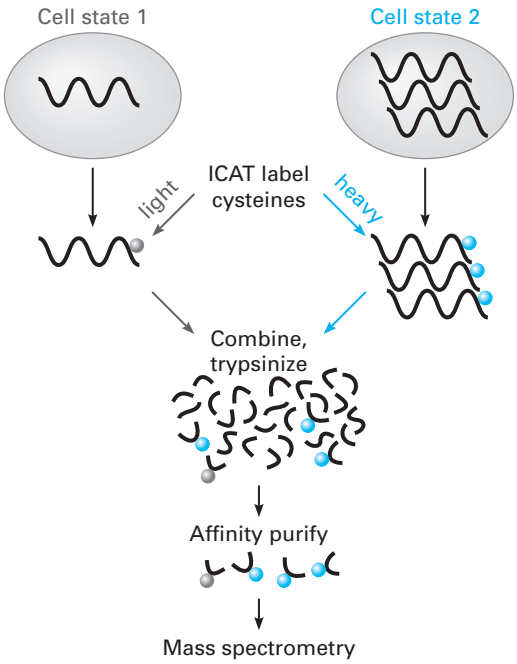

FIGURE 6.28 • Schematic of ICAT method. Proteins from two cell populations are labeled with either the heavy (blue) or light (gray) ICAT reagent. The proteins are isolated, mixed, and digested with trypsin. ICAT-labeled peptide fragments are affinity purified and analyzed by tandem MS.

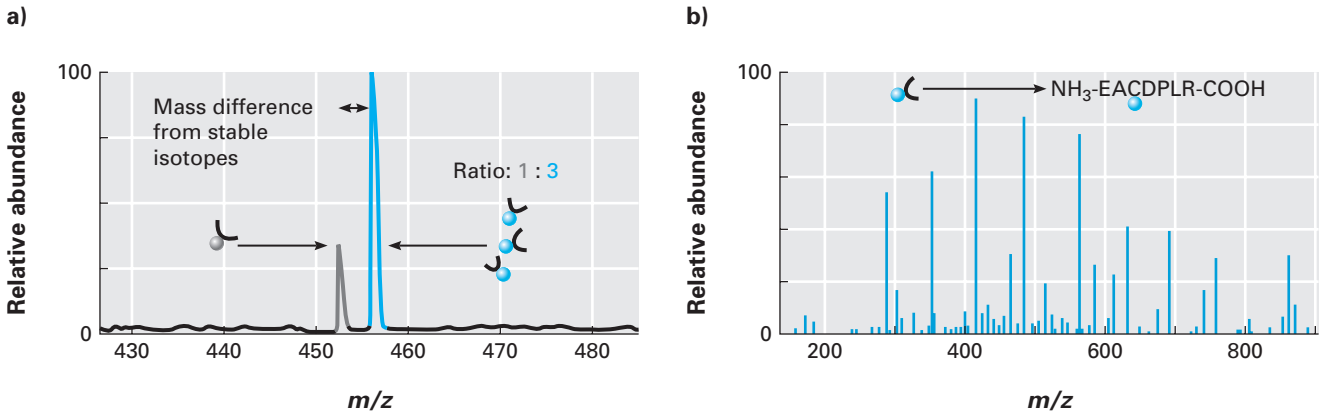

FIGURE 6.29 • Quantification and identification of proteins by ICAT. **a)** The heavy (blue) and light (gray) peptides are separated and quantified to produce a ratio for each protein from the two different cell populations. **b)** Each peptide bound to an ICAT reagent is subjected to MS analysis. Protein identification is performed by determining the amino acid sequence of the peptide and comparing it to a database of all possible trypsin fragments from the yeast proteome.

FIGURE 6.30 • Reversible metabolic pathway for ethanol and galactose utilization. The major proteins and products are shown. The two alcohol dehydrogenases are indicated as Adh1 and Adh2.

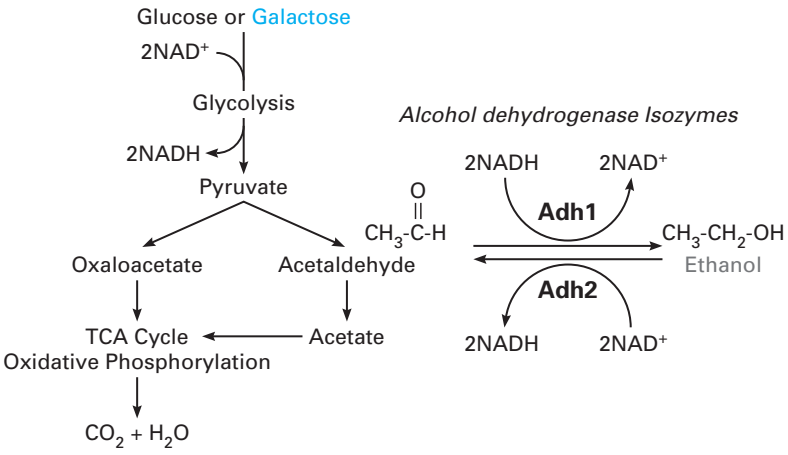

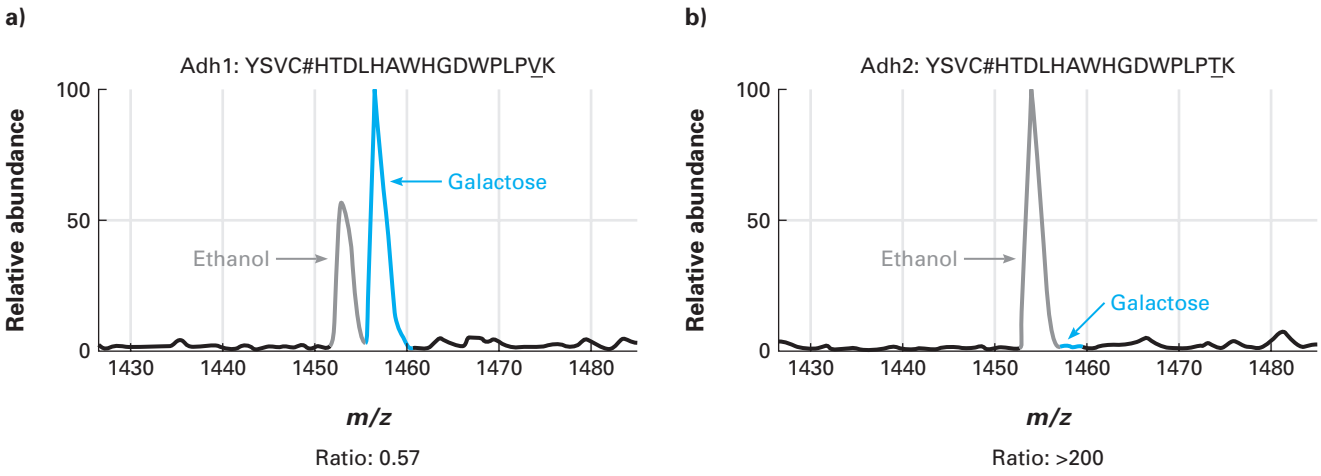

FIGURE 6.31 • Reversible switch in metabolism. ICAT detection of **a)** Adh1 and **b)** Adh2 from yeast cells grown in the presence of ethanol (gray) or galactose (blue). Relative amounts of these two proteins are indicated with ratios at the bottom.

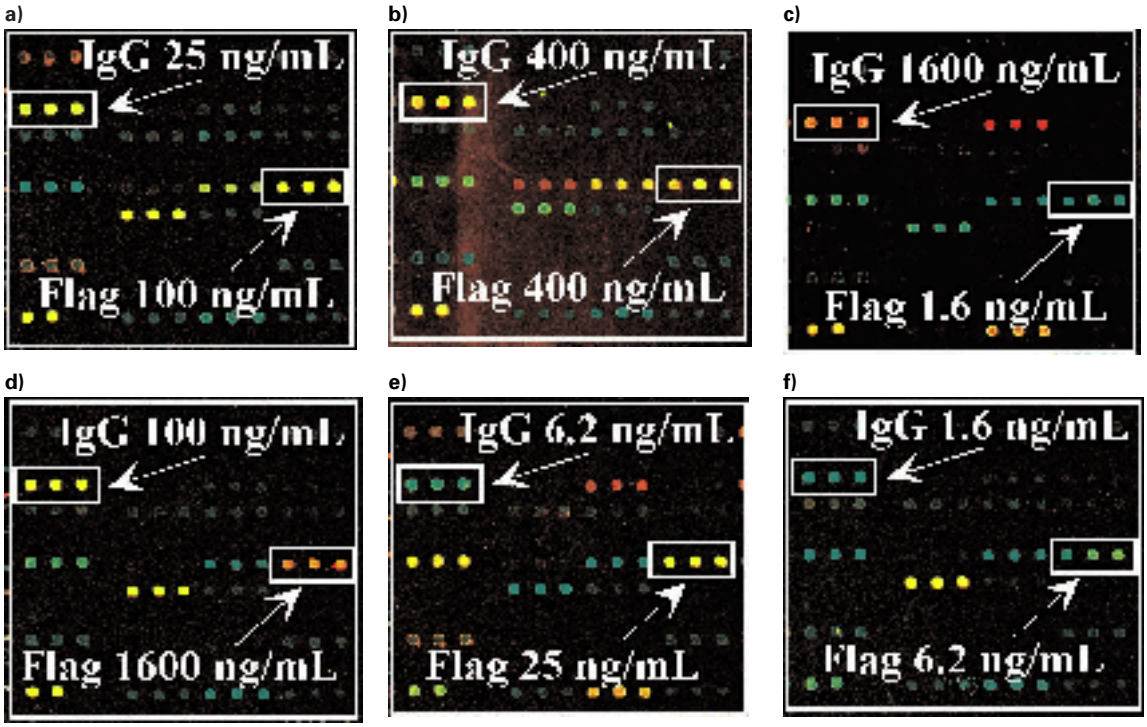

FIGURE 6.32 • Antibody arrays detected fluorescently labeled antigens. Two of the 115 different antibody/antigen pairs are shown in this montage: the Flag protein and IgG protein used as antigens. The labels indicate the concentration of the antigen applied to each array.

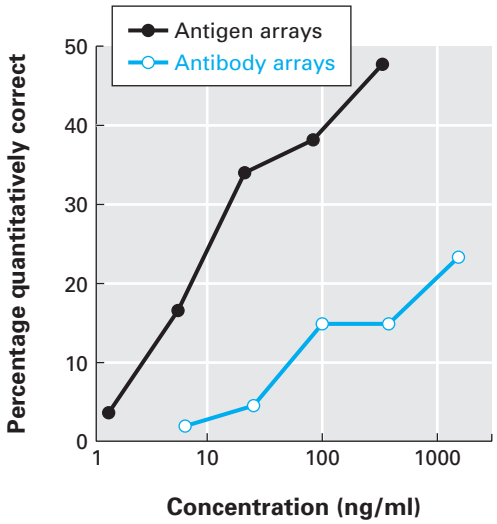

FIGURE 6.33 • Comparison of two protein microarrays. Percentages of antibodies and antigens yielding quantitatively correct results when known protein mixtures were incubated on protein microarrays.

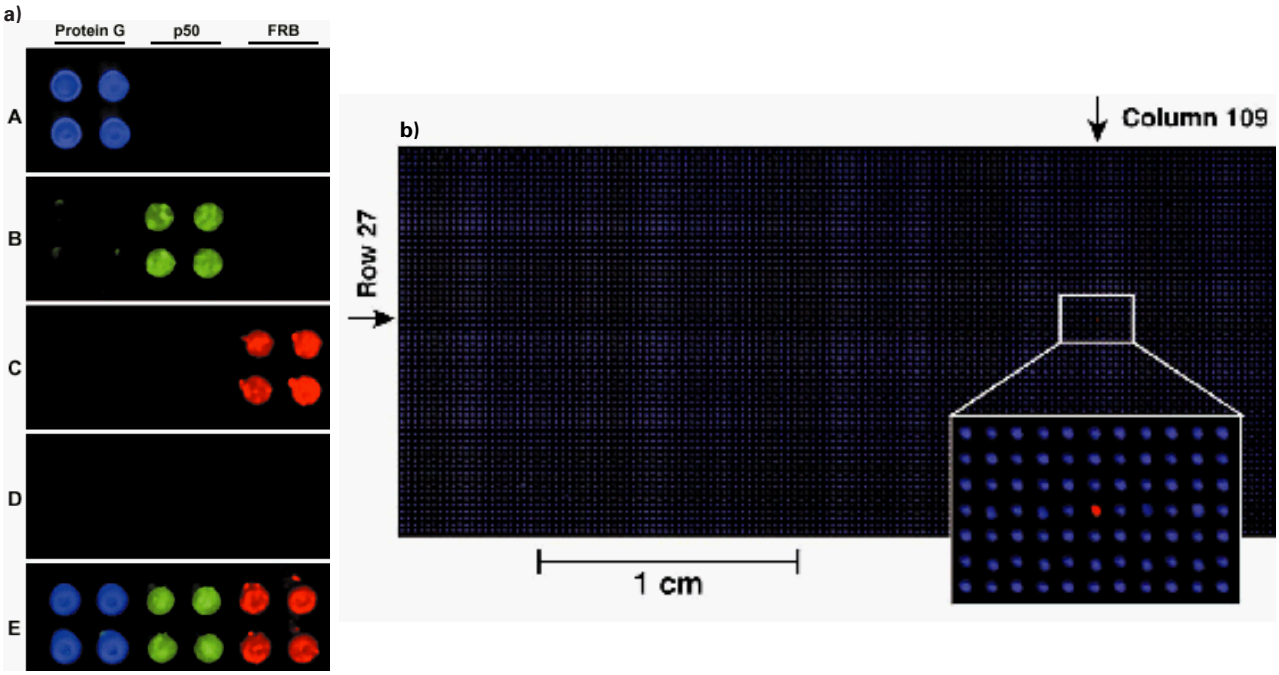

FIGURE 6.34 • Detection of protein-protein interactions on protein microarrays.
a) The slide was spotted with the three proteins listed at the top. Slide A was probed with fluorescent IgG antibody. Slide B was probed with fluorescent IκBα. Slide C was probed with fluorescent FKB binding protein plus rapamycin, which is required for FRB-FKBP interaction. Slide D was probed with FKBP in the absence of rapamycin. Slide E was probed with all three proteins that were labeled with different color dyes. **b)** Detection of one target in 10,800 features. Protein G was spotted 10,799 times, and a single FRB feature was printed in row 27, column 109. The slide was probed with blue labeled IgG and red FKBP in the presence of rapamycin.

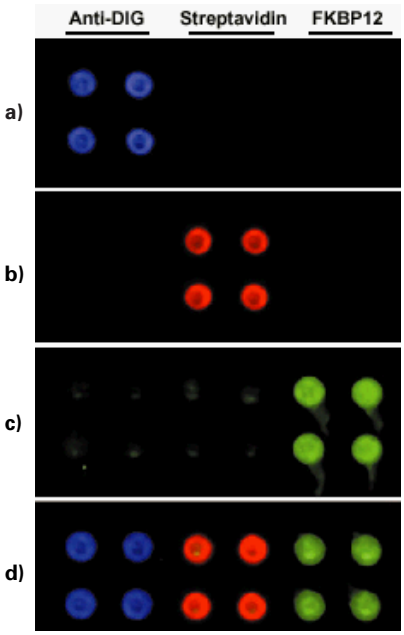

FIGURE 6.35 • Detecting the targets of small molecules on protein arrays. The microarrays were created by spotting anti-DIG antibody, avidin (which binds to biotin), and FKBP (which binds to AP1497). Slide **a)** was probed with the epitope tag DIG bound to a protein and a blue dye. Slide **b)** was probed with biotin bound to a protein and a red dye. Slide **c)** was probed with AP1497 bound to a protein and a green dye. Slide **d)** was probed with a mixture of all three.

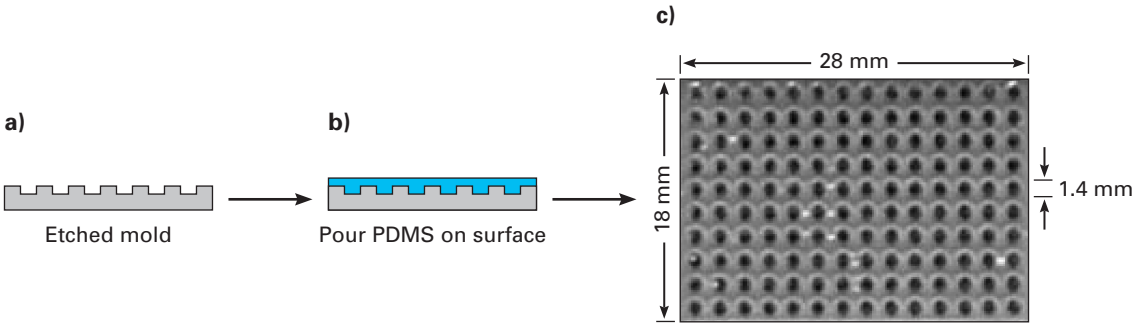

FIGURE 6.36 • Microwell array manufacturing. **a)** Molds were etched, and then **b)** monomeric elastomer was used to form a silicon-based polymer (blue). **c)** When removed from the mold, an array of microwells was produced and ready for the next step.

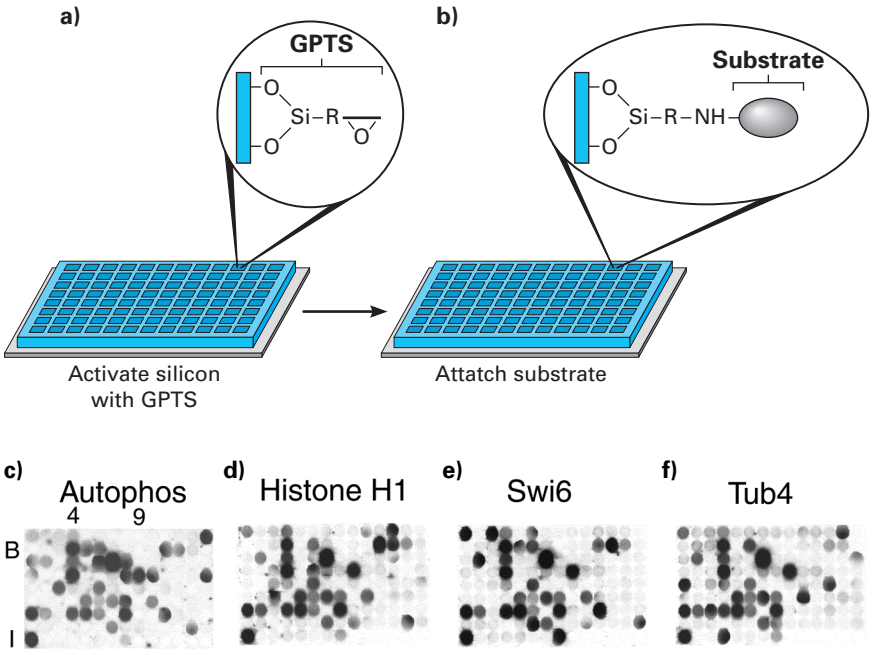

FIGURE 6.37 • Coupling substrate to the array of microwells.
a) The silicon polymer was activated with a crosslinker called 3-glycidoxypropyltrimethoxysilane (GPTS).
b) The peptides used as substrates were covalently linked to the silicon.
c) to **f)** Four of the 119 kinase microwell assays are shown in this figure. Each microwell array contained one substrate (labeled at the top) while a different kinase and radioactive ATP (^{33}Pγ-ATP) were added to each microwell. The microwell arrays were imaged with a sensitive device called a phosphoimager.

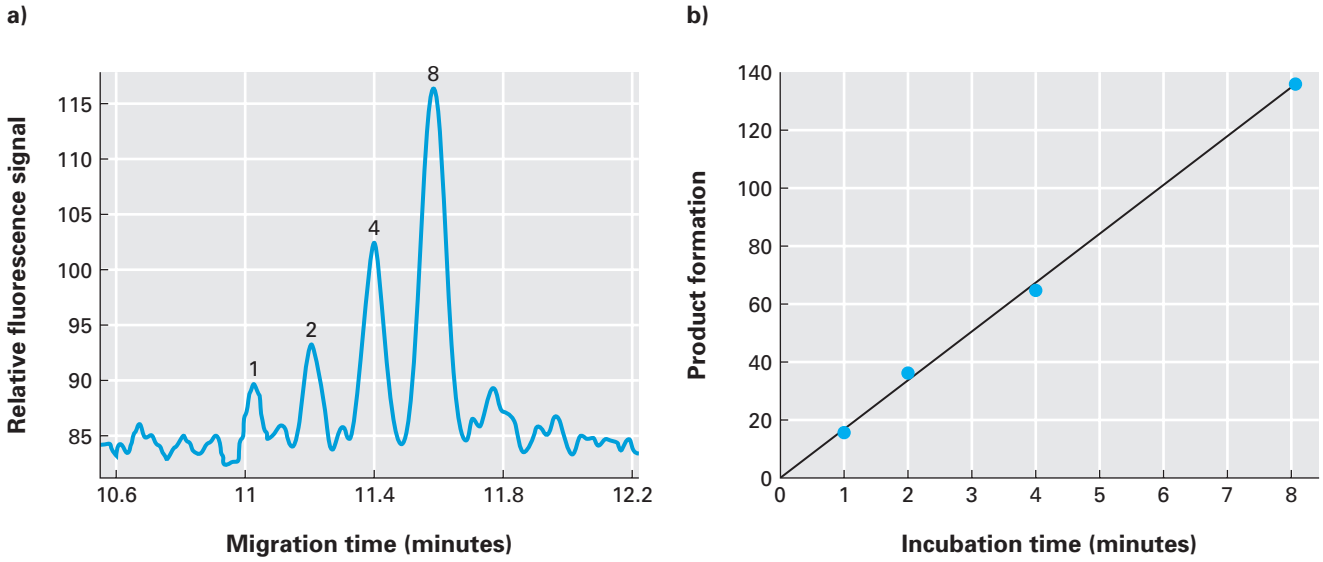

FIGURE 6.38 • Measuring the rate of product formation from a single enzyme molecule. **a)** Product formation generated by reacting a single enzyme for 1, 2, 4, and 8 minutes. **b)** Kinetic plot of the data from a). The amounts of product for each incubation time are shown and the straight line is the least-squares fit to the data. Correlation coefficient is 0.999.

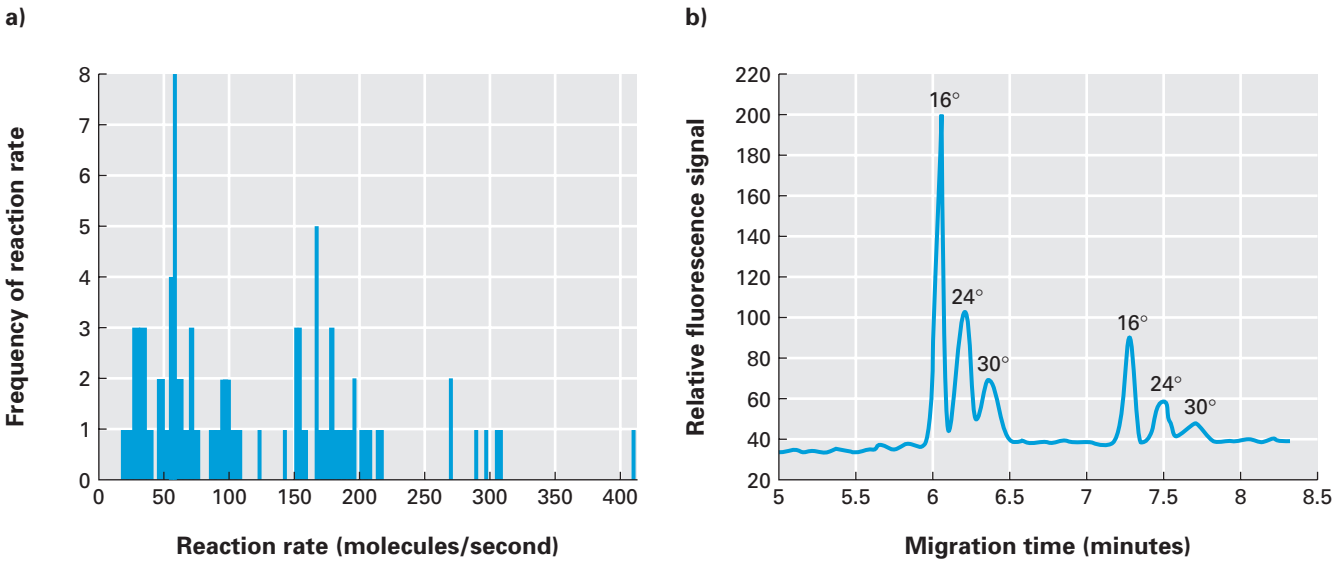

FIGURE 6.39 • Variation between enzymes. **a)** Histogram of reaction rates observed for 83 different alkaline phosphatase molecules assayed individually. Activity was determined from the incubation time and product formation. **b)** Electropherogram of alkaline phosphatase assay using two different molecules. Each molecule was incubated sequentially at 16°C, 24°C, and 30°C.

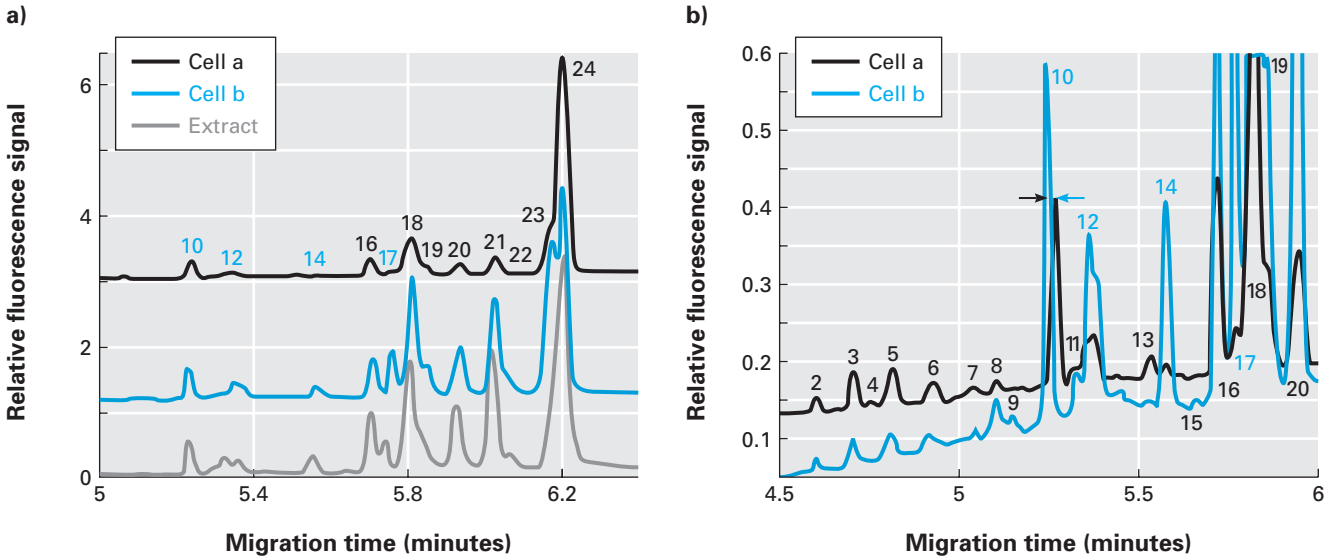

FIGURE 6.40 • Capillary electrophoresis of single-cell proteomes. **a)** Two individual human colon adenocarcinoma cells (blue and black; cell line HT29) were subjected to one-dimensional separation. The "extract" was produced from approximately 10^6 cells (gray). Only the major peaks are labeled. **b)** Higher resolution of the central portion of a). The arrows mark differences in migration times between the two number 10 peaks.

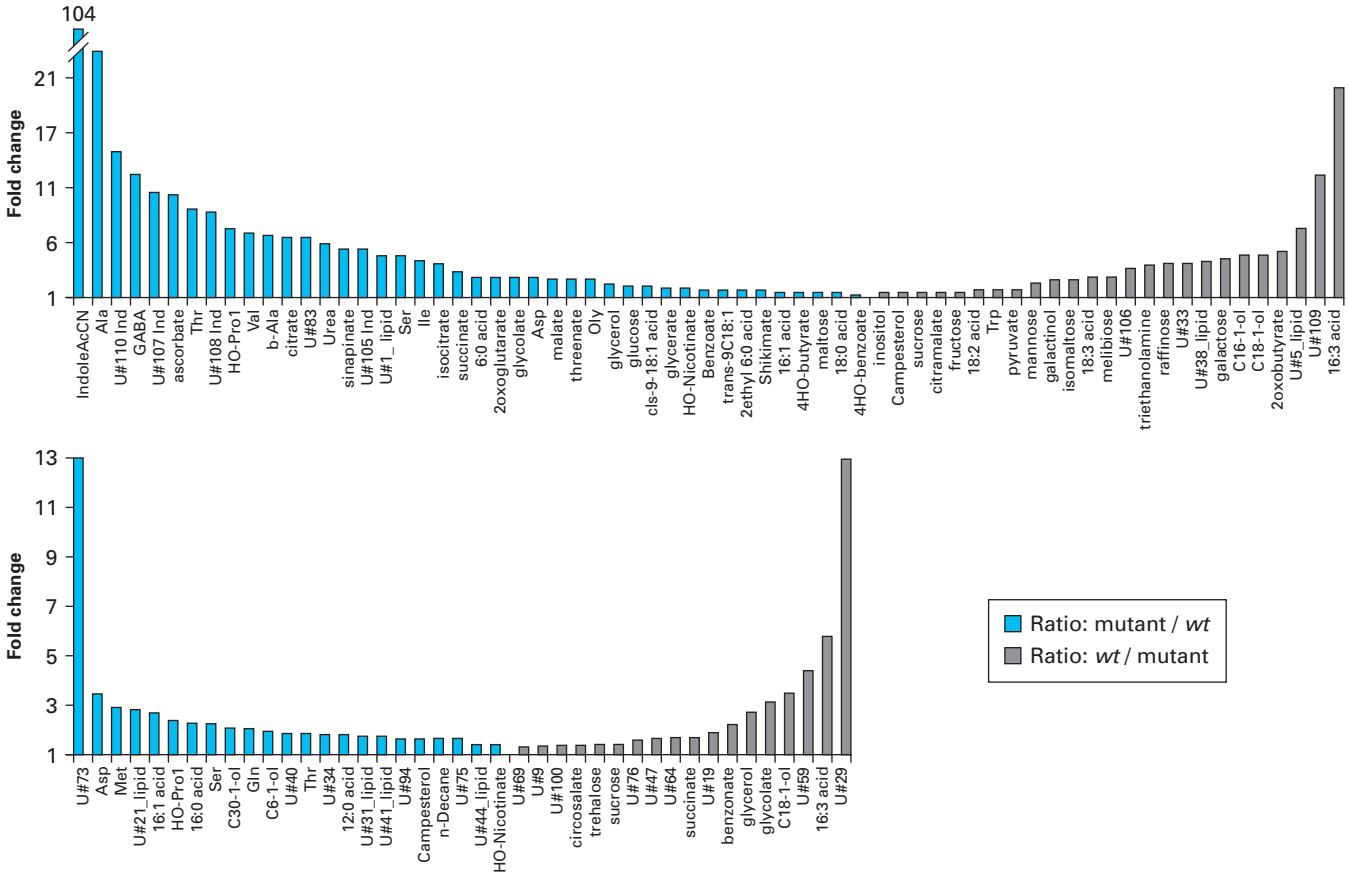

FIGURE 6.41 • Significant changes in metabolomes when comparing *wt* to mutant strains. **a)** Alteration in average metabolite levels (*t*-test *p*-value < 0.01) of Dgd1 compared to its parental strain Col-2. Only 67 of the 153 significant differences detected are shown. **b)** When compared to its parental strain (C-24), Sdd1-1 had 41 significant differences in its metabolome; all 41 are shown.